SUPPLEMENTAL INFORMATION

Methods

Patient sample collection and use.

All patient samples were obtained following informed consent from the Cardiothoracic Surgery Department, Weill Cornell Medical College (New York). Specimens were collected after obtaining written informed consent prior to undergoing any study-specific procedures in accordance with the Declaration of Helsinki. Patient identity for pathological specimens remained anonymous in the context of this study. Patient sample collection was approved by the Institutional Review Board of Weill Cornell Medical College; Thoracic Surgery Biobank Protocol Number 1008011221.

Human tissue immunostaining, histology, and microscopy.

Resected tissue was washed with Hank's Balanced Salt Solution, fixed in 4% paraformaldehyde overnight at 4°C, dehydrated in 30% sucrose overnight at 4°C, embedded in a 2:1 ratio of OCT (O. C. T. Compound, Tissue-Tek): 30% sucrose, and flash-frozen on dry ice. Blocks were stored at -80°C. 8-10 μm-thick sections were cut on a cryostat microtome (Leica CM3050 S, Leica Biosystems) and mounted on slides (VWR Micro Slides Superfrost Plus, VWR North American).

For immunofluorescence staining, sections (10 μm) were fixed in cold acetone for 10 minutes and incubated with a blocking buffer (5% FBS and 0.1% Triton in PBS) for 1 hour. Sections were then stained following a standard protocol with antibodies against EpCAM, CD45, and PD-L1. Fluorescence images were obtained using a computerized

Zeiss fluorescence microscope (Axiovert 200M), fitted with an apotome and a HRM camera. Images were analyzed using Axiovision 4.6 software (Carl Zeiss Inc.).

For immunohistochemical staining, selected sections from human lung cancer and adjacent normal lung were stained for CD3 using standard protocols. Briefly, sections were pre-treated using heat-mediated antigen retrieval with Tris-EDTA buffer (pH 9, epitope retrieval solution 2) for 20 minutes. Sections were then incubated with PA0553 for 15 minutes at room temperature and detected using an HRP conjugated compact polymer system. 3,3 diaminobenzidine tetrachloride (DAB) was used as the chromogen. Finally, sections were counterstained with hematoxylin and mounted with Leica Micromount. Images were acquired using an Olympus BX43 microscope and a Jenoptik ProgRes CF camera.

For hematoxylin and eosin staining, 4 μm-thick formalin-fixed, paraffin-embedded tissue sections were stained using a Leica staining module (Buffalo Grove, IL) and following a standard protocol. Briefly, sections were deparaffinized using xylenes, hydrated through sequential washes of 100% ethanol, 95% ethanol, 70% ethanol, and water; stained with hematoxylin; washed in water; cleaned with acid alcohol to remove excess hematoxylin; washed in water; hematoxylin blued with lithium carbonate; washed in water; stained with eosin; sequentially dehydrated with 95% ethanol and 100% ethanol; cleared with Histoclear; and coverslipped with Leica Micromount. Images were acquired using an Olympus BX43 microscope and a Jenoptik ProgRes CF camera.

Human sample flow cytometry staining and analysis.

Resected tissue was minced and digested in a collagenase and DNAse solution in Hank's Balanced Salt Solution (HBSS, Gibco), and incubated at 37°C for 30 minutes on a rotator. Digested tissue was subsequently passed through a 70 μm cell strainer, and red blood cells lysed with RBC Lysis Buffer (5PRIME) in HBSS on ice for 10 minutes. Cells were pelleted at 3,000 rpm for 10 minutes, resuspended in HBSS, passed through a 40 μm cell strainer, pelleted again, washed twice with FACS Buffer, and resuspended in FACS Buffer. Samples were incubated with antibodies for 30 minutes on ice, washed with FACS Buffer, and resuspended in FACS Buffer. Samples were acquired on a Becton-Dickinson FACS Aria II sorter and analyzed using FlowJo 10 (FlowJo, LLC).

Animal work.

All animal work was performed in accordance with an animal protocol approved by the institutional Animal Care and Use Committee at WCMC (Protocol number 0806-762A). Female C57BL/6J (catalogue number 000664) mice were purchased from The Jackson Laboratory (Bar Harbor, Maine).

Spontaneous KP model.

KRAS$^{LSL\text{-}G12D/+}$; *TP53*$^{flox/flox}$ (KP) mice were generated as described previously (1), and confirmed by genotyping using standard protocols. At 12-15 weeks of age, these mice were intratracheally administered 2-3 x 10^4 lentiviral particles expressing Cre recombinase and luciferase as described (1). Tumor growth was monitored by BLI (see below) and lungs were harvested beginning 10 weeks post lentiviral administration for analysis.

Orthotopic HKP1 model.

HKP1 lung cancer cells derived from KP tumor lungs and expressing mCherry-Luciferase (1) were maintained in DMEM supplemented with 10% FBS, penicillin/streptomycin, and L-glutamine (complete DMEM). 150,000 HKP1 cells suspended in sterile PBS were administered via the tail vein into syngeneic female 8-week-old C57BL/6J mice. Tumor growth in vivo was evaluated twice weekly via bioluminescence imaging (BLI). Briefly, mice were anesthetized with isoflurane and administered 75mg/kg D-luciferin (Promega) retro-orbitally. Tumor growth was monitored using a Xenogen IVIS system coupled to Living Image acquisition and analysis software (Living Image; Xenogen), with mice in a supine position after D-luciferin injection. For BLI plots, photon counts were calculated for each mouse by using the same circular region of interest encompassing the thorax of the mouse.

Mouse treatment studies.

HKP1 lung cancer cells expressing mCherry-Luciferase were administered orthotopically using the protocol described above. At day 6 post-administration, BLI data were collected and mice were grouped such that similar mean tumor burdens were present in each treatment cohort. Mice were injected intraperitoneally with 250μg of anti-PD-1 or IgG2a control on days 6, 10, 13, and 17 post-implantation (or on days 7, 10, 13, and 16 for RNA-Seq experiments). For survival studies, mouse tumor burden was evaluated bi-weekly, and mice were euthanized when tumor burden reached humane endpoints. Separate cohorts of mice were sacrificed on day 18 (1 day after the last dose of

anti-PD-1 or IgG2a) and analyzed via IF, H&E, or flow cytometry, or on day 14, day 17, and day 24 in the RNA-Seq experiments. For depletion studies, mouse tumor burden was evaluated on day 6 post-implantation, and mice were grouped such that similar mean tumor burdens were present in each treatment cohort. On day 6, mice were treated with either: 400μg of anti-CD4 + 400μg of IgG2b, 400μg of anti-CD8a + 400μg of IgG2b, 400μg of anti-CD4 + 400μg of anti-CD8a, or 800μg of IgG2b ; mice were subsequently treated with half-doses of antibody or IgG2b control on days 9, 12, and 15. Submandibular bleeds were performed on days 7 and 16 to confirm depletion efficiency. Mice with depletion of T cell subsets were subsequently treated with 250μg of anti-PD-1 on days 7, 10, 13, and 16; the two groups of mice treated with IgG2b control were subsequently treated with 250μg of anti-PD-1. Mouse tumor burden was evaluated bi-weekly via BLI imaging.

Mouse tissue immunostaining and microscopy.

At specified time points, mice were euthanized and perfused with PBS. Lungs were post-fixed in 1% formaldehyde overnight at 4°C, dehydrated in 30% sucrose overnight at 4°C, embedded in a 2:1 ratio of OCT (O. C. T. Compound, Tissue-Tek): 30% sucrose, and flash-frozen on dry ice. Blocks were stored at -80°C. 8-10 μm-thick sections were cut on a cryostat microtome (Leica CM3050 S, Leica Biosystems) and mounted on slides (VWR Micro Slides Superfrost Plus, VWR North American).

For immunofluorescence staining, sections (10 μm) were fixed in cold acetone for 10 minutes and incubated with a blocking buffer (5% FBS and 0.1% Triton in PBS) for 1 hour. Sections were then stained following a standard protocol with antibodies against E-

Cadherin, CD45, PD-1, PD-L1, CD4, and CD8. Fluorescence images were obtained using a computerized Zeiss fluorescence microscope (Axiovert 200M), fitted with an apotome and a HRM camera. Images were analyzed using Axiovision 4.6 software (Carl Zeiss Inc.).

For hematoxylin and eosin staining, sections were hydrated through sequential washes of 100% ethanol, 95% ethanol, 70% ethanol, and water; stained with hematoxylin; washed in water; cleaned with acid alcohol to remove excess hematoxylin; washed in water; hematoxylin blued with lithium carbonate; washed in water; stained with eosin; sequentially dehydrated with 95% ethanol and 100% ethanol; cleared with Histoclear; and coverslipped with Cytoseal. Images were acquired on an Olympus BX40F-3 microscope with an Olympus DP26 camera.

Mouse tissue flow cytometry staining.

At specified time points, mice were euthanized and perfused with PBS. Lungs were then dissected, diced, and ground through a 140 μm wire mesh (Cell Screen/100mesh, Bellco Glass, Inc.) into RPMI-1640 supplemented with 10% FBS, penicillin/streptomycin, L-glutamine, non-essential amino acids, sodium pyruvate, and β -mercaptoethanol (complete RPMI). Single-cell suspensions were subsequently filtered through 70 μm filters (Cell Strainer, 70 micron, Nylon; Falcon) and centrifuged for 5 minutes at 1,500 rpm. Cell pellets were resuspended in 1mL ACK Lysing Buffer (QualityBiological) for one minute for red blood cell lysis, neutralized with 9mLs complete RPMI, and centrifuged for 5 minutes at 1,500 rpm. Cell pellets were washed

once with FACS Buffer (PBS supplemented with 0.5% Bovine Serum Albumin and 2mM EDTA), centrifuged for 5 minutes at 1,500 rpm, and resuspended in FACS Buffer.

For surface stains, samples were subsequently blocked with anti-mouse CD16/32 for 15 minutes at room temperature, incubated with primary antibodies for 30 minutes on ice in the dark, washed with FACS Buffer, post-fixed with 1% formaldehyde for 30 minutes on ice in the dark, washed with FACS Buffer, and resuspended in FACS Buffer. Samples were covered in aluminum foil and stored at 4°C until analysis (less than 24 hours later).

For intracellular stains, if they required stimulation, samples were stimulated using PMA (100ng/mL) and ionomycin (1μg/mL) for 4 hours in complete RPMI at 37°C in a humidified incubator. Golgi blocking was achieved via treatment with Brefeldin A (Biolegend) and Monensin (Biolegend) for 4 hours in complete RPMI at 37°C in a humidified incubator. Samples were subsequently blocked with anti-CD16/32 for 15 minutes at room temperature, incubated with primary antibodies for surface stains for 30 minutes on ice in the dark, washed with FACS Buffer, fixed with Fixation/Permeabilization Buffer (eBioscience) for 30 minutes on ice in the dark, washed with Permeabilization Buffer (eBioscience), incubated with primary antibodies for intracellular stains in Permeabilization Buffer for 30 minutes on ice in the dark, washed 3 times with Permeabilization Buffer, and resuspended in FACS Buffer. Samples were covered in aluminum foil and stored at 4°C until analysis (less than 24 hours later).

Data were acquired on either a Becton-Dickinson FACSCalibur Cytek DxP11 or a Becton-Dickinson LSR II and analyzed with FlowJo 10 (FlowJo, LLC).

Mouse submandibular bleed flow cytometry staining.

At specified time points, peripheral blood was collected via submandibular jaw bleeds from each mouse into K2EDTA Microtainers (BD Biosciences, Catalogue #365974). Blood was subsequently diluted in balanced salt solution, and viable lymphocytes isolated using Ficoll-Paque PLUS (GE Healthcare, Catalogue #17144003) following the manufacturer's instructions. Cell suspensions were centrifuged for 5 minutes at 1,500 rpm to form pellets, washed once with FACS Buffer (PBS supplemented with 0.5% Bovine Serum Albumin and 2mM EDTA), centrifuged for 5 minutes at 1,500 rpm, and resuspended in FACS Buffer.

Samples were subsequently blocked with anti-mouse CD16/32 for 15 minutes at room temperature, incubated with fluorescence-conjugated antibodies against CD45, CD3, CD4, and CD8 for 30 minutes on ice in the dark, washed with FACS Buffer, post-fixed with 1% formaldehyde for 30 minutes on ice in the dark, washed with FACS Buffer, and resuspended in FACS Buffer. Samples were covered in aluminum foil and stored at 4°C until analysis (less than 24 hours later).

Data were acquired on a Becton-Dickinson FACSCelesta and analyzed with FlowJo 10 (FlowJo, LLC).

Mouse tissue lung-infiltrating T cell sorting, RNA extraction, and RNA-Seq analysis.

At specified time points, mice were euthanized and perfused with PBS. Lungs were then dissected, diced, and ground through a 140 μm wire mesh (Cell Screen/100mesh, Bellco Glass, Inc.) into RPMI-1640 supplemented with 10% FBS, penicillin/streptomycin, L-glutamine, non-essential amino acids, sodium pyruvate, and β

-mercaptoethanol (complete RPMI). Single-cell suspensions were subsequently filtered through 70 μm filters (Cell Strainer, 70 micron, Nylon; Falcon) and centrifuged for 5 minutes at 1,500 rpm. Cell pellets were resuspended in 1mL ACK Lysing Buffer (QualityBiological) for one minute for red blood cell lysis, neutralized with 9mLs complete RPMI, and centrifuged for 5 minutes at 1,500 rpm. Cell pellets were washed once with FACS Buffer (PBS supplemented with 0.5% Bovine Serum Albumin and 2mM EDTA), centrifuged for 5 minutes at 1,500 rpm, and resuspended in FACS Buffer.

Samples were subsequently blocked with anti-mouse CD16/32 for 15 minutes at room temperature, incubated with primary antibodies for 30 minutes on ice in the dark, washed with FACS Buffer, stained with DAPI for 10 minutes at 0.2 μ g/mL, washed with FACS Buffer, and resuspended in FACS Buffer. Samples were sorted on a Becton-Dickinson FACS Aria II sorter, and $DAPI^-$ $CD3^+$ $CD4^+$ $CD8^-$ cells ($CD4^+$ T cells) and $DAPI^-$ $CD3^+$ $CD4^-$ $CD8^+$ cells ($CD8^+$ T cells) were sorted into RLT lysis buffer supplemented with β-mercaptoethanol (RNeasy Mini Kit, Qiagen). RNA was subsequently using these kits with on-column DNA digestion as per the manufacturer's protocols.

cDNA libraries were generated using the Illumina TruSeq RNA Sample Preparation kit and sequenced with single-end 50 bps on HiSeq4000 sequencer. Tophat2 (2) was used to align raw sequencing reads to the mm9 mouse reference genome. Cufflinks (3, 4) was used to measure transcript abundances in Fragments Per Kilobase of exon model per Million mapped reads (FPKM) with upper-quartile normalization and sequence-specific bias correction. Inter-sample relationships within the CD4 and CD8 datasets were evaluated by principal component analysis in R (5) and visualized using

ggplot (6). Differential gene expression was assessed by utilizing the limma package (7), with pairwise comparisons of BLI Groups 2, 3, 4, 5, and 6 relative to IgG treated mice, following the standard protocol. Significance cutoff values were set at $\log_2$ fold-change >1, p-value <0.05 and false discovery rate <10%. Heatmaps were made using the pheatmap (https://CRAN.R-project.org/package=pheatmap) and RColorBrewer (https://CRAN.R-project.org/package=RColorBrewer) packages after normalizing $\log_2$-transformed FPKM values by the maximum FPKM value for each transcript, and the Venny web portal was used to make all Venn diagrams (http://bioinfogp.cnb.csic.es/tools/venny/index.html). Figure 7 heatmaps were generated by intersecting the differential gene expression lists from all pairwise comparisons with a list of transcriptional regulators, co-inhibitory and co-stimulatory molecules, and cytokines and chemokines and their cognate receptors associated with exhaustion from (8). We employed the GSE30431 dataset, which contains transcriptome data from naïve, memory, effector, and exhausted $CD4^+$ and $CD8^+$ T cells, in order to generate molecular signatures of significantly up/down regulated genes for all pairwise comparisons using the same cutoffs as the prior analyses. These signatures were separated into their respective up and down components and used as the gene sets to perform a Gene Set Enrichment Analysis (GSEA, standard parameters, (9)) to evaluate the phenotypic status of our 5 anti-PD-1 treated groups relative to IgG. In order to evaluate gene ontologies in the dataset, the significance cutoffs were altered to absolute $\log_2$ fold-change >0.5, p-value <0.05 and false discovery rate <20%, for all pairwise comparisons; genes identified with this altered cutoff are indicated in Table S3 in red. Differentially expressed genes were mapped to entrez identifiers with the org.Mm.eg.db package (org.Mm.eg.db) and

subsequently analyzed using the GOstats package (10), where significance was evaluated by computing the Hypergeometric P-values for representation of each GO term.

Whole exome sequencing and analysis.

Tissue for whole exome sequencing analyses was obtained from grossly visible nodules or regions known to contain tumor by BLI. At specified time points, mice were euthanized and perfused with PBS. Lungs were then dissected and diced, while germline DNA was extracted from blood in the inferior vena cava. DNA was extracted using the DNeasy kit (Qiagen) and submitted for sequencing. Library preparation was performed using the SureSelect kit (Agilent). 8 samples were run on the HiSeq4000 (Illumina) with Paired-End clustering and 100x2 cycles.

Whole exome sequencing data (SureSelect) was aligned to mouse genome build mm10 using the Burrows-Wheeler Aligner (http://bio-bwa.sourceforge.net). Picard tools (https://broadinstitute.github.io/picard/) were used to mark and remove duplicates and fix mates in the aligned BAM files. The Genome Analysis Toolkit (GATK) was used to realign around insertions or deletions (InDels) and to recalibrate the BAMs (https://software.broadinstitute.org/gatk/). The GATK was also used to perform quality control on the final BAMs files, especially to check for average read depth in the regions covered by SureSelect.

The somatic single-nucleotide variants (SNVs) in the paired tumor-normal samples were identified using MuTect, Strelka, and VarScan, and the SNVs identified by at least 2 mutation callers were retained. InDels were identified using Strelka and VarScan and those identified by both tools were retained. The identified somatic alterations were further filtered using the following criterion: (a) read depth for both

tumor and matched normal samples is ≥ 30 reads, (b) the variant allele frequency (VAF) in tumor samples is ≥ 5%, (c) the VAF of matched normal samples is ≤ 1%, (d) at least 5 reads supporting the alteration in the tumor samples. SNVs and Indels were annotated using Variant Effect Predictor (http://www.ensembl.org/info/docs/tools/vep/index.html).

The human lung adenocarcinoma (LUAD) MuTect mutation calls and clinical annotations were downloaded from the GDC (https://portal.gdc.cancer.gov, access date 05/18/2017). For the purpose of the comparative analysis, the samples that did not belong to either stage I or II LUAD were excluded. In addition, the samples that did not have both mutation call and clinical annotations available were excluded, resulting in 398 LUAD samples. The LUAD samples were classified as smokers if the patient had clinical information related to cigarettes per day or years smoked, else classified as non-smokers. R software package was used for plots.

Statistical analysis.

Results are expressed as mean ± SEM. Analyses of different time points in untreated tumor progression were performed using one- or two-way ANOVAs with Tukey's multiple comparisons test. Analyses of different treatment groups were performed using the Log-Rank Mantel-Cox test for survival and two-tailed *t*-tests corrected for multiple comparisons when appropriate using the Holm-Sidak method, using the GraphPad Prism statistical program. P values < 0.05 were considered significant.

Accession numbers.

The RNA Sequencing data are available in the Gene Expression Omnibus database (http://www.ncbi.nlm.nih.gov/gds) under the accession number GSE114300. Whole Exome Sequencing data are available in the BioProject database (http://www.ncbi.nlm.nih.gov/bioproject) under the project number PRJNA470948.

Antibodies and Recombinant Proteins Used

Use	Species	Antibody	Clone	Company	Dilution/ Concentration
Flow Cytometry	Mouse	anti-CD3	17A2	Biolegend	1:100
Flow Cytometry	Mouse	anti-CD4	RM4-5	Biolegend	1:100
Flow Cytometry	Mouse	anti-CD8a	53-6.7	Biolegend	1:100
Flow Cytometry	Mouse	anti-CD8b	YTS156.7.7	Biolegend	1:100
Flow Cytometry	Mouse	anti-CD11b	M1/70	Biolegend	1:100
Flow Cytometry	Mouse	anti-CD11c	N418	Biolegend	1:100
Flow Cytometry	Mouse	anti-CD44	IM7	Biolegend	1:100
Flow Cytometry	Mouse	anti-CD45	30-F11	Biolegend	1:100
Flow Cytometry	Mouse	anti-CD62L	MEL-14	Biolegend	1:100
Flow Cytometry	Mouse	anti-FoxP3	FJK-16s	eBioscience	1:40
Flow Cytometry	Mouse	anti-Ki67	11F6	Biolegend	1:100
Flow Cytometry	Mouse	anti-PD-1	29F.1A12	Biolegend	1:100
Flow Cytometry	Mouse	anti-Gr-1	RB6-8C5	Biolegend	1:100
Flow Cytometry	Mouse	anti-IDO	2E2/IDO1	Biolegend	1:100
Flow Cytometry	Mouse	anti-NOS2	CXNFT	eBioscience	1:100
Flow Cytometry	Mouse	anti-TNFa	MP6-XT22	Biolegend	1:100
Flow Cytometry	Mouse	anti-IFNg	XMG1.2	Biolegend	1:100
Flow Cytometry	Mouse	anti-GzmB	GB11	Biolegend	1:100
Flow Cytometry	Mouse	anti-Tbet	4B10	Biolegend	1:100
Flow Cytometry	Mouse	anti-Eomes	Dan11mag	eBioscience	1:100
Flow Cytometry	Mouse	anti-TIM-3	RMT3-23	Biolegend	1:100
Flow Cytometry	Mouse	anti-TIGIT	Vstm3	Biolegend	1:100
Flow Cytometry	Mouse	anti-CTLA-4	UC10-4B9	Biolegend	1:100
Flow Cytometry	Mouse	anti-LAG-3	C9B7W	Biolegend	1:100
Flow Cytometry	Mouse	anti-2B4	m2B4 (B6)458.1	Biolegend	1:100
Flow Cytometry	Human	anti-CD3	OKT3	Biolegend	1:200
Flow Cytometry	Human	anti-CD4	A161A1	Biolegend	1:200
Flow Cytometry	Human	anti-CD8	SK1	Biolegend	1:200
Flow Cytometry	Human	anti-PD-1	EH12.2H7	Biolegend	1:200
Flow Cytometry	Human	anti-PD-L1	29E.2A3	Biolegend	1:200
Flow Cytometry	Human	anti-EpCAM	9C4	Biolegend	1:200
In vivo neutralization	Mouse	anti-PD-1	RMP1-14	BioXCell	250ug/dose
In vivo neutralization	Mouse	IgG2a	2A3	BioXCell	250ug/dose
In vivo depletion	Mouse	anti-CD4	GK1.5	BioXCell	200-400ug/dose

In vivo depletion	Mouse	anti-CD8a	2.43	BioXCell	200-400ug/dose
In vivo depletion	Mouse	IgG2b	LTF-2	BioXCell	200-400ug/dose
Immunofluorescence	Mouse	anti-E-Cadherin	DECMA1	Biolegend	1:40
Immunofluorescence	Mouse	anti-CD45	30-F11	Biolegend	1:25
Immunofluorescence	Mouse	anti-PD-1	RMP1-30	eBioscience	1:25
Immunofluorescence	Mouse	anti-PD-L1	10F.9G2	Biolegend	1:25
Immunofluorescence	Mouse	anti-CD4	RM4-5	Biolegend	1:40
Immunofluorescence	Mouse	anti-CD8	53-6.7	Biolegend	1:25
Immunofluorescence	Human	anti-EpCAM	9C4	Biolegend	1:25
Immunofluorescence	Human	anti-CD45	HI30	Biolegend	1:25
Immunofluorescence	Human	anti-PD-L1	29E.2A3	Biolegend	1:25
Immunohistochemistry	Human	anti-CD3	LN10	Leica	

Supplemental Figure Legends

Supplemental Figure 1: Sample gating and representative data for PD-1 positivity in human tissue samples (n=9 each for tumor and adjacent tissue). (A) T cells are gated on CD3-positivity and EpCAM-negatively, then positively gated for CD8 or CD4. (B) Sample plot showing $CD8^+$ (blue) and $CD4^+$ (red) T cells, with quadrangle gates showing $PD\text{-}1^+$ portions of the populations.

Supplemental Figure 2: Representative bioluminescence imaging (BLI) data from the orthotopic HKP1 mouse lung cancer model. 150,000 HKP1 cells in sterile PBS were injected intravenously via the tail vein, and BLI imaging performed at 1 week, 2 weeks, and 3 weeks post-implantation. Data from 60 seconds of acquisition (week 1) or 20 seconds of acquisition (weeks 2 and 3) are shown on the left; corresponding matched BLI values are shown on the plot on the right. n=8. BLI values for weeks 2 and 3 were normalized to 60 seconds of acquisition by multiplying the acquired values by 3; acquisition times were reduced at weeks 2 and 3 due to saturation of signal because of higher tumor burdens.

Supplemental Figure 3: PD-1 expression on tumor-infiltrating T cells in the orthotopic HKP1 mouse lung cancer model. Representative immunofluorescence stains of tumor-bearing lung tissue 1 week (upper panels) and 3 weeks (lower panels) post-implantation for: (A) DAPI (blue), E-Cadherin (white), CD4 (green), and CD8 (red); (B) DAPI (blue), E-Cadherin (red), PD-1 (green), and CD4 (white); and (C) DAPI (blue), E-Cadherin

(red), PD-1 (green), and CD8 (pink). Tumor regions are labeled with T; adjacent tissue is labeled with A. Staining was performed on 3 samples. Scale bar: 100μm. Scale bars for immunofluorescence stains are shown on the images themselves.

Supplemental Figure 4: PD-1 expression on T cell subsets isolated from tumor-bearing lungs. Flow cytometric analysis of tumor-bearing lung tissue 1 week (blue dots), 2 weeks (red dots), and 3 weeks (green dots) post-implantation for PD-1 mean fluorescence intensity in $CD4^+$ ($CD3^+$ $CD4^+$), Th ($CD3^+$ $CD4^+$ $FoxP3^-$), Treg ($CD3^+$ $CD4^+$ $FoxP3^+$), and $CD8^+$ ($CD3^+$ $CD8^+$) T cell populations. n=7-8 per group. Statistics: Two-way ANOVA with Tukey's multiple comparisons test. NS non-significant, *$p<0.05$, ***$p<0.001$, **** $p<0.0001$.

Supplemental Figure 5: Emergence of expression of other checkpoints and exhaustion-related transcriptional regulators at later time points post-implantation in the orthotopic HKP1 mouse lung cancer model. Representative contour plots for $CD4^+$ (red contour plots) and $CD8^+$ (blue contour plots) T lymphocytes localized in naïve lung tissue (Naïve), tumor-bearing lung tissue 1 week post-implantation (Early), and tumor-bearing lung tissue 3 weeks post-implantation (Late). Cells were analyzed for expression of (A) 2B4, CTLA-4, and TIGIT, n=4-5 per group; (B) TIM-3 and LAG-3, n=4-5 per group; and (C) Eomes and T-Bet, n=12-16 per group, via flow cytometry.

Supplemental Figure 6: Emergence of expression of other checkpoints and exhaustion-related transcriptional regulators at later time points post-implantation in the orthotopic

HKP1 mouse lung cancer model. Flow cytometric analysis of naïve lung tissue (black dots) or tumor-bearing lung tissue 1 week (blue dots) or 3 weeks (green dots) post-implantation for mean fluorescence intensity of (A) CTLA-4, TIGIT, and 2B4, n=4-5 per group; (B) TIM-3 and LAG-3, n=4-5 per group; and (C) Eomes and T-Bet, n=12-16 per group, via flow cytometry. Statistics: (A-C) Two-way ANOVAs with Tukey's multiple comparisons test. NS non-significant, * $p<0.05$, *** $p<0.001$, **** $p<0.0001$.

Supplemental Figure 7: Myeloid cell accumulation and functional alteration over time in the orthotopic HKP1 mouse lung cancer model. Flow cytometric analysis of tumor-bearing lung tissue 1 week (blue dots), 2 weeks (red dots), and 3 weeks (green dots) post-implantation for (A) myeloid cell population proportions, (B) myeloid cell IDO mean fluorescence intensity, and (C) myeloid cell NOS2 mean fluorescence intensity. n=7-8 per group. Statistics: (A-C) Two-way ANOVAs with Tukey's multiple comparisons test. NS non-significant, * $p<0.05$, ** $p<0.01$, *** $p<0.001$, **** $p<0.0001$.

Supplemental Figure 8: Anti-PD-1 therapy initiated early in tumor progression results in surpressed tumor growth kinetics but with a wide range of responses. (A, B) Bioluminescence imaging (BLI) data measuring tumor growth in IgG-treated (red lines) or anti-PD-1-treated (blue lines) mice from the top-most quartile of tumor burden (A) or the bottom-most quartile of tumor burden (B). Black symbols indicate the last time point at which a given mouse was imaged before euthanasia or mortality. n=5 per group in each chart of a total 20 mice per treatment arm.

Supplemental Figure 9: Enhanced PD-1 expression on Th and Treg cells, corresponding with dysfunctional Treg IFNγ production. (A, B) Flow cytometric analysis of tumor-bearing lung tissue from mice treated with IgG (red dots) or anti-PD-1 (blue dots) for (A) mean fluorescence intensity of PD-1 in $CD4^+$ ($CD3^+$ $CD4^+$), Th ($CD3^+$ $CD4^+$ $FoxP3^-$), Treg ($CD3^+$ $CD4^+$ $FoxP3^+$), and $CD8^+$ ($CD3^+$ $CD8^+$) T cell populations, and (B) frequency of PD-1^+ and PD-1^- Tregs in the total Treg population or the total $CD4^+$ T cell population. (C) Sample flow cytometry contour plots examining IFNγ production in PD-1^+ and PD-1^- Tregs from mice treated with IgG (red contour plots, left panel) or anti-PD-1 (blue contour plots, right panel). n=7 per group. Statistics: (A, B) Two-tailed unpaired t-tests with Holm-Sidak correction for multiple comparisons. NS non-significant, * $p<0.05$, ** $p<0.01$, *** $p<0.001$.

Supplemental Figure 10: Analysis of other immune phenotypes for alterations by anti-PD-1 treatment. (A, B) Flow cytometric analysis of tumor-bearing lung tissue from mice treated with IgG (red dots) or anti-PD-1 (blue dots) for mean fluorescence intensity of GzmB, IL-2, and FasL in $CD4^+$ (A) and $CD8^+$ (B) T cells, normalized to the mean fluorescence intensity of the same in IgG-treated mice. n=5-7 per group. (C) Flow cytometric analysis of tumor-bearing lung tissue from mice treated with IgG (red dots) or anti-PD-1 (blue dots) for T central memory (Tcm, $CD44^+$ $CD62L^+$) and T effector and T effector memory (Teff + Tem, $CD44^+$ $CD62L^-$). n=7 per group. (D) Flow cytometric analysis of tumor-bearing lung tissue from mice treated with IgG (red dots) or anti-PD-1 (blue dots) for myeloid cell population proportions. n=7 per group. (E, F) Flow cytometric analysis of tumor-bearing lung tissue from mice treated with IgG (red dots) or

anti-PD-1 (blue dots) for (E) myeloid cell IDO mean fluorescence intensity, and (F) myeloid cell NOS2 mean fluorescence intensity. n=7 per group. Statistics: (A-F) Two-tailed unpaired t-tests with Holm-Sidak correction for multiple comparisons. NS non-significant, * $p<0.05$, ** $p<0.01$, *** $p<0.001$.

Supplemental Figure 11: Efficacious antibody-mediated depletion of T cell subsets. Sample flow cytometry contour plots demonstrating depletion of targeted T cell subsets in peripheral blood on days 7 (left panels) and 16 (right panels) post-implantation. n=8-10 per group.

Supplemental Figure 12: Depletion of T cell subsets alters anti-PD-1-mediated tumor growth control. (A-D) Bioluminescence imaging (BLI) data measuring tumor growth in anti-PD-1-treated mice with depletion of: (A) no T cell subsets (blue lines); (B) $CD8^+$ T cells (green lines); (C) $CD4^+$ T cells (purple lines); or (D) $CD8^+$ and $CD4^+$ T cells (black lines). Reductions in BLI readings at day 20 in several mice in panel (D) were due to excessive tumor burden. Red arrow in panel (C) indicates the mouse that had depletion of $CD4^+$ T cells on day 16 but not on day 7. n=8-10 per group.

Supplemental Figure 13: Differential exhaustion-associated gene expression in Groups with different growth and treatment phenotypes. (A-C) Heatmaps for gene expression in co-inhibitory and co-stimulatory molecules (A), transcriptional regulators (B), and cytokines and chemokines and their cognate receptors associated with exhaustion (8)

between the 6 groups in indicated cell types. Statistics: (A-C) Moderated t-statistic from the limma package, with Benjamini and Hochberg's adjustment for multiple testings.

Supplemental Figure 14: Differential expression of subset-specific transcription factors in $CD4^+$ T cells in Groups with different growth and treatment phenotypes. Heatmap for gene expression of transcription factors specific to the indicated subsets between the 6 groups.

Supplemental Figure 15: Overlaps of significantly differently expressed genes compared with IgG in different groups. Venn diagrams of genes significantly differentially expressed compared with IgG in Groups 2, 4, and 5 (top row), and in Groups 3, 6, and 5 (bottom row) in $CD4^+$ T cells (left panels) and $CD8^+$ T cells (right panels). Significant differences in gene expression were determined by $\log_2$ fold change > 1, $p<0.05$, and adjusted $p<0.1$. Statistics: Moderated t-statistic from the limma package, with Benjamini and Hochberg's adjustment for multiple testings.

Supplemental Figure 16: Accumulation of PD-1+ T cells in human tumor specimens throughout early-stage disease. (A, B) Flow cytometric analysis for $PD\text{-}1^+$ percentages of $CD4^+$ (A) and $CD8^+$ (B) T lymphocytes from paired tumor and adjacent tissue from early-stage human lung cancer patients, divided by stage. Stage IA: n=4; stage IB: n=3; stage IIA: n=1, stage IIIA: n=1.

Supplemental Figure 17: Enhanced mutational load closer to that observed in human patients in the HKP1 orthotopic model compared with the adenoviral LSL-$Kras^{G12D}$

$p53^{fl/fl}$ (spontaneous) model, which does not recruit T cells. (A, B) Whole exome sequencing was performed on tumors isolated from the orthotopic and spontaneous models, and mutational analysis performed. These results were compared with those identified in stage I and II tumors from The Cancer Genome Atlas Lung Adenocarcinoma (TCGA-LUAD) data collection in aggregate (A) or separated by smoking status (B). Data are presented as box and whisker plots. n=2 spontaneous tumors, n=2 orthotopic tumors, n=115 stage I and II non-smokers, and n=283 stage I and II smokers.

Supplemental Figure 18: IFNγ and TNFα production in both $CD4^+$ and $CD8^+$ T cells inversely correlate with tumor burden in anti-PD-1-treated mice. (A, B) IFNγ, TNFα, IL-2, and FasL mean fluorescence intensity was plotted against bioluminescence imaging (BLI) data normalized to values taken pre-treatment measuring tumor growth in anti-PD-1-treated mice. Individual values for 13 mice were plotted and linear regressions calculated in $CD4^+$ (A) and $CD8^+$ (B) T cells. Statistics: P value testing for null hypothesis that slope is 0. * $p<0.05$, ** $p<0.01$.

Supplemental References

1. Choi H et al. Transcriptome Analysis of Individual Stromal Cell Populations Identifies Stroma-Tumor Crosstalk in Mouse Lung Cancer Model. *CellReports* 2015;10(7):1187–1201.
2. Kim D et al. TopHat2: accurate alignment of transcriptomes in the presence of insertions, deletions and gene fusions. *Genome Biol.* 2013;14(4):R36.
3. Trapnell C et al. Transcript assembly and quantification by RNA-Seq reveals unannotated transcripts and isoform switching during cell differentiation. *Nat. Biotechnol.* 2010;28(5):511–515.
4. Trapnell C et al. Differential analysis of gene regulation at transcript resolution with RNA-seq. *Nat. Biotechnol.* 2013;31(1):46–53.
5. R Core Team (2017). R: A language and environment for statistical computing. R Foundation for Statistical Computing, Vienna, Austria.
6. Wickham H. ggplot2: Elegant Graphics for Data Analysis. Springer-Verlag New York, 2009.
7. Ritchie ME et al. limma powers differential expression analyses for RNA-sequencing and microarray studies. *Nucleic Acids Res.* 2015;43(7):e47.
8. Crawford A et al. Molecular and Transcriptional Basis of $CD4^+$ T Cell Dysfunction during Chronic Infection. *Immunity* 2014;40(2):289–302.
9. Mootha VK et al. PGC-1alpha-responsive genes involved in oxidative phosphorylation are coordinately downregulated in human diabetes. *Nat Genet* 2003;34(3):267–273.
10. Falcon S, Gentleman R. Using GOstats to test gene lists for GO term association.

Bioinformatics 2007;23(2):257–258.

Supplemental Figure 1

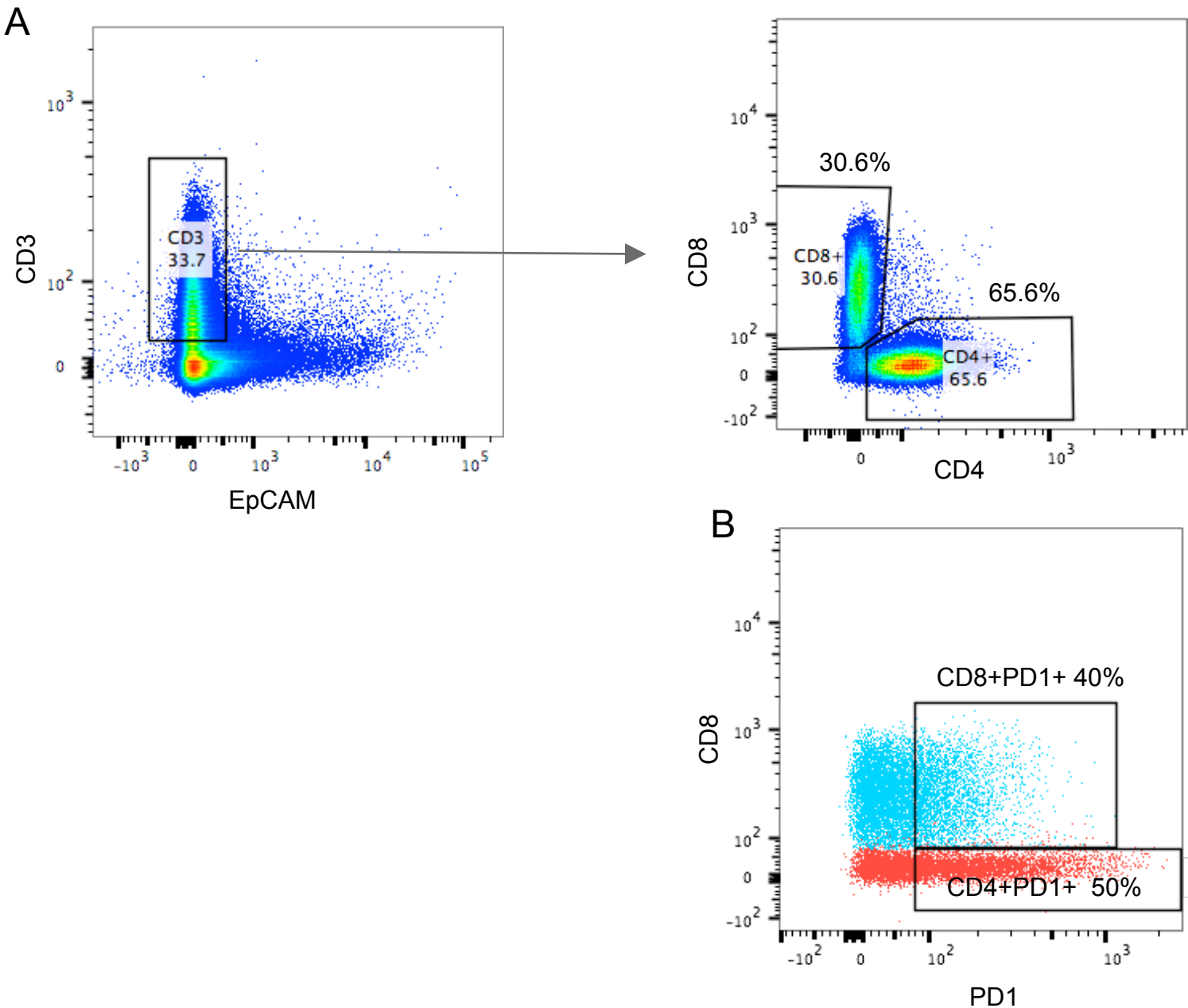

Supplemental Figure 2

Week 1
60s. Exposure

Week 2
20s. Exposure

Week 3
20s. Exposure

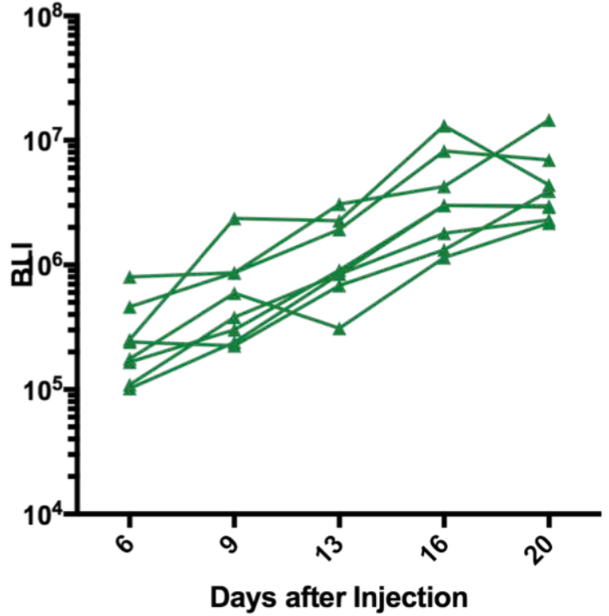

Supplemental Figure 3

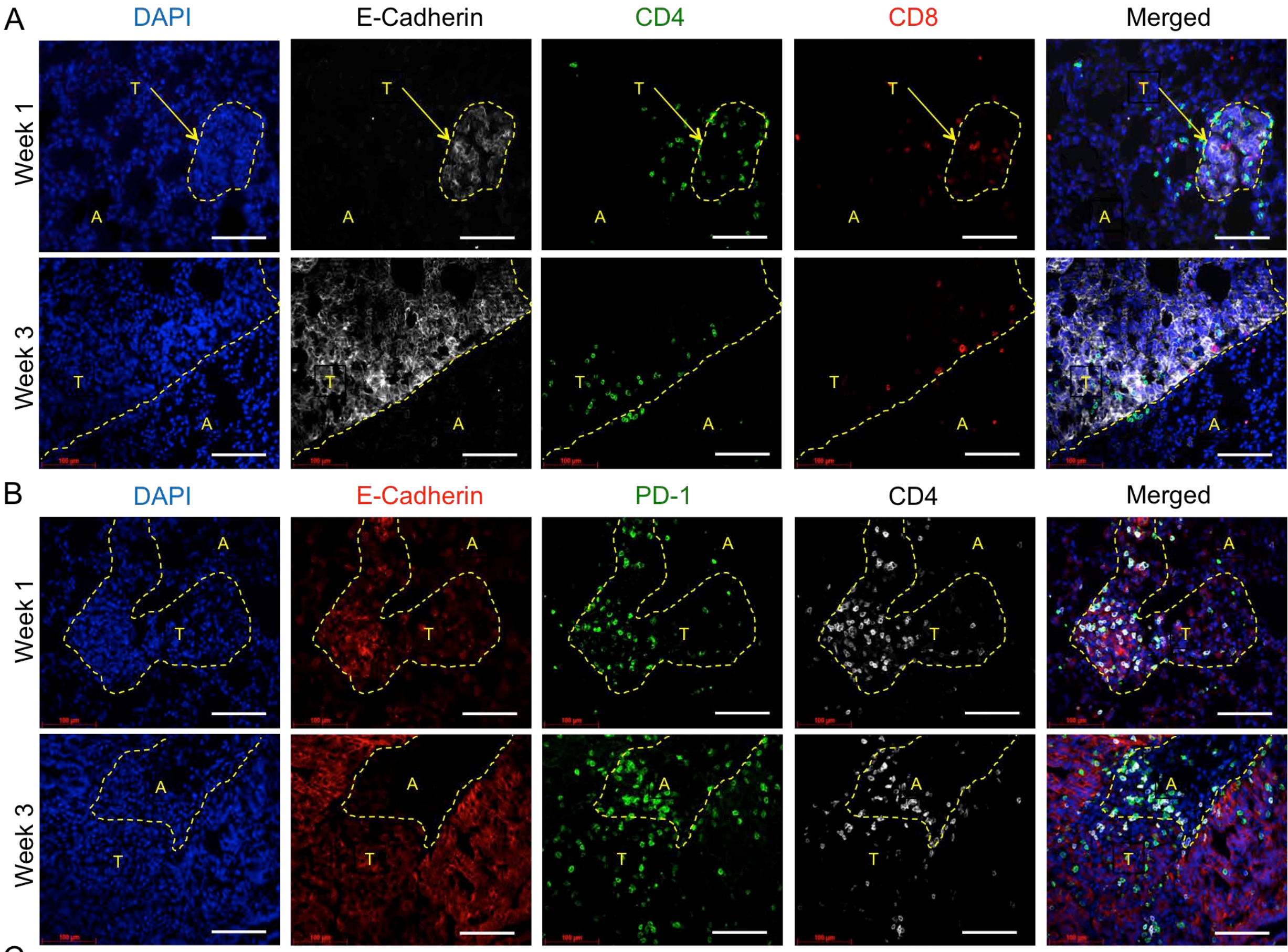

Supplemental Figure 4

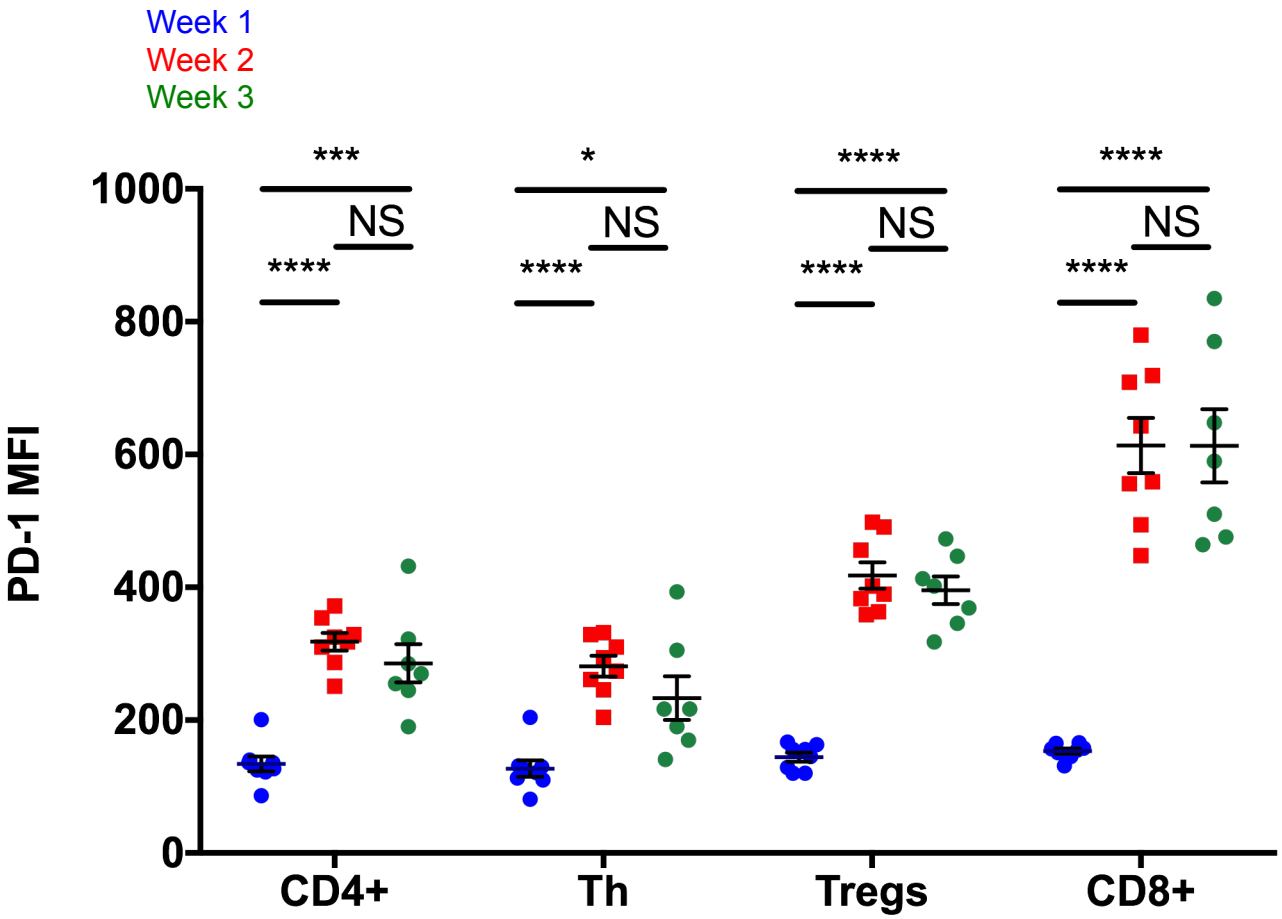

Supplemental Figure 5

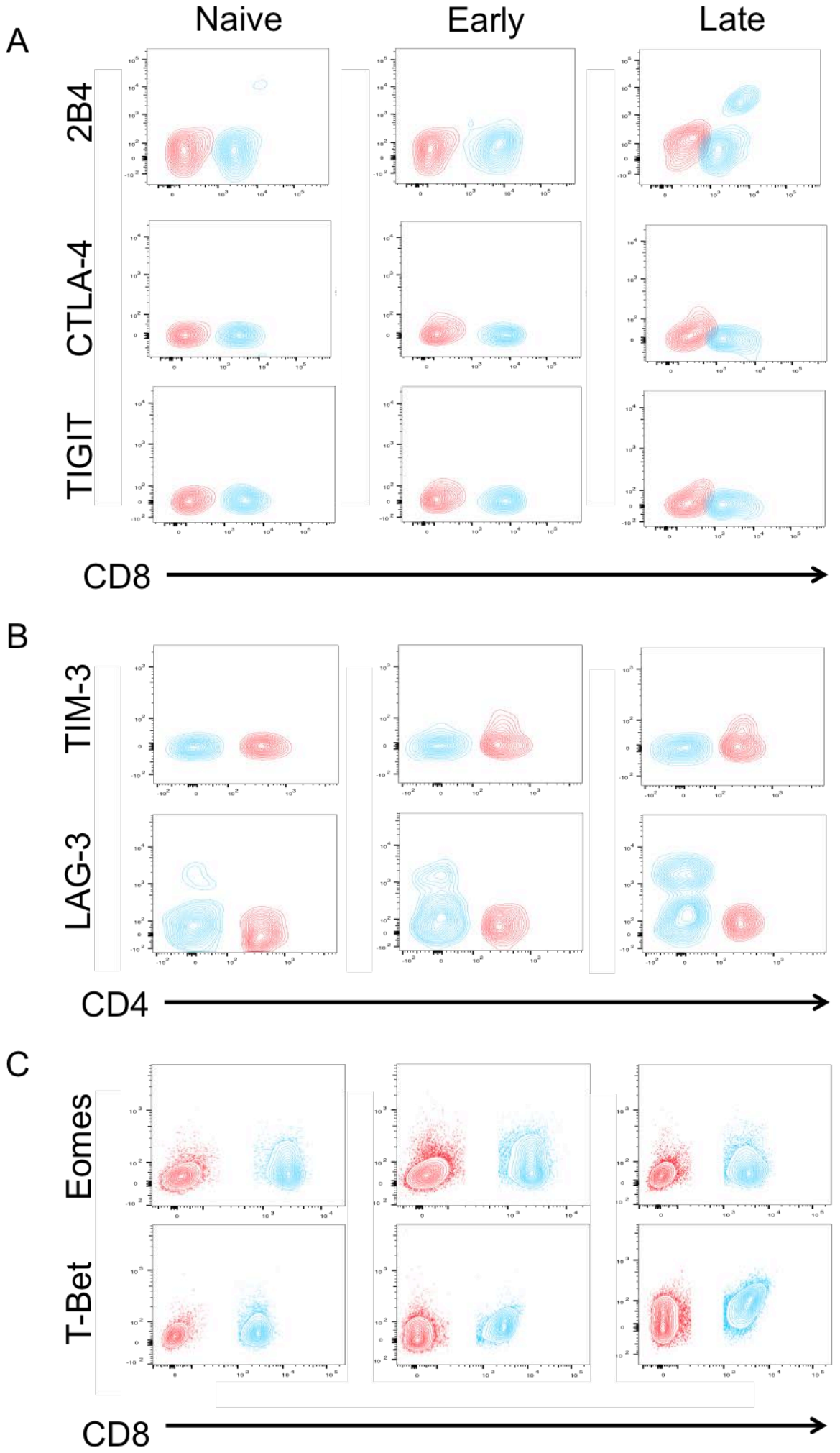

Supplemental Figure 6

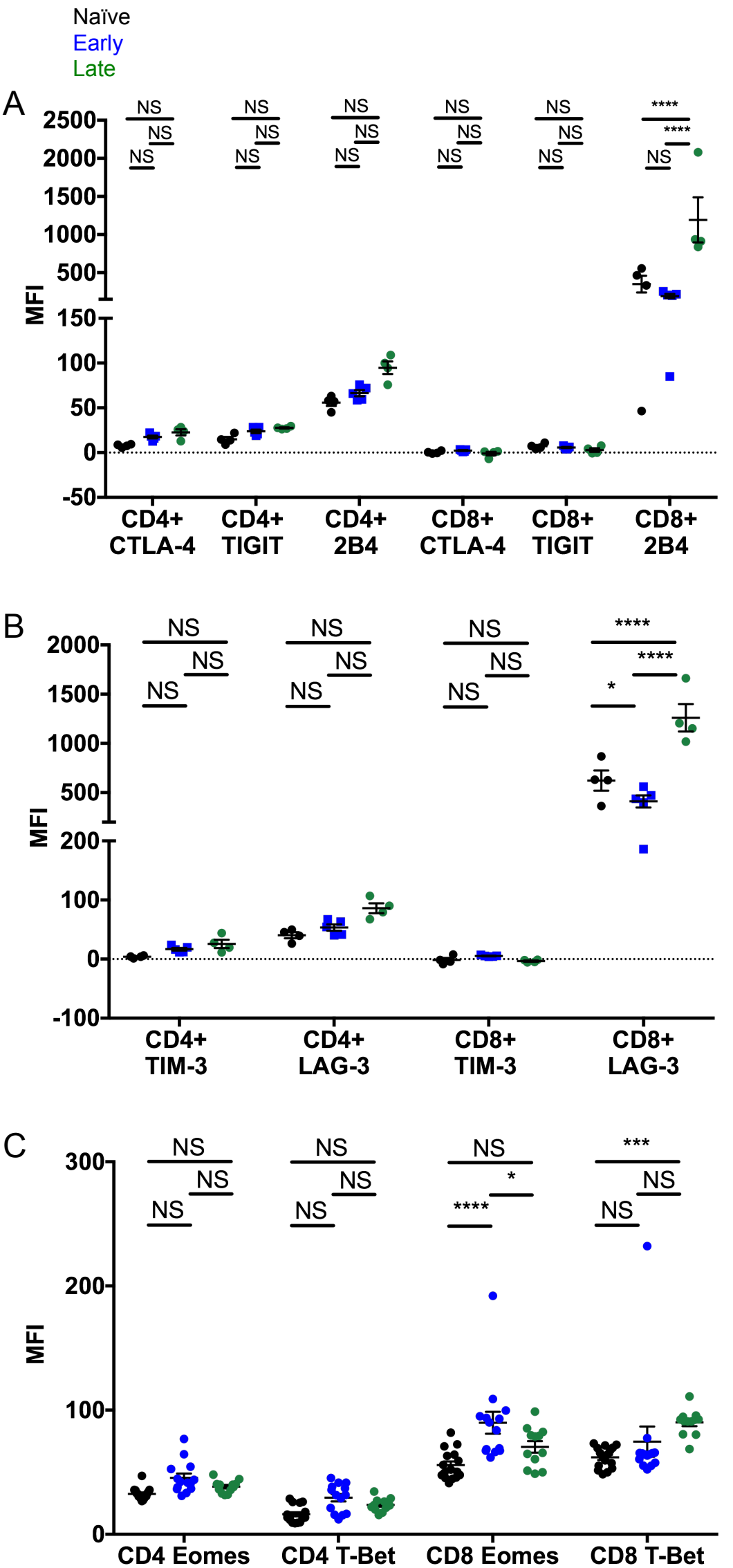

Supplemental Figure 7

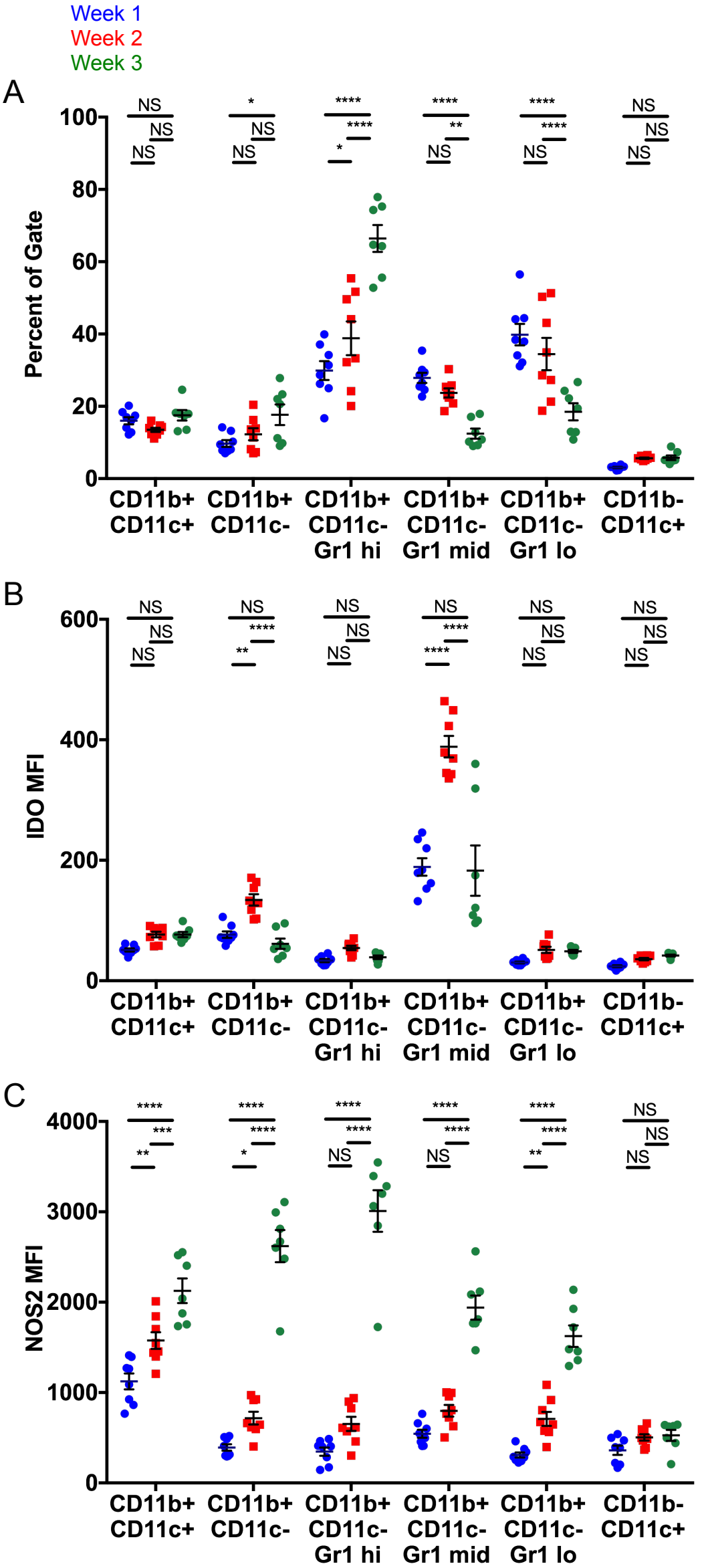

Supplemental Figure 8

A

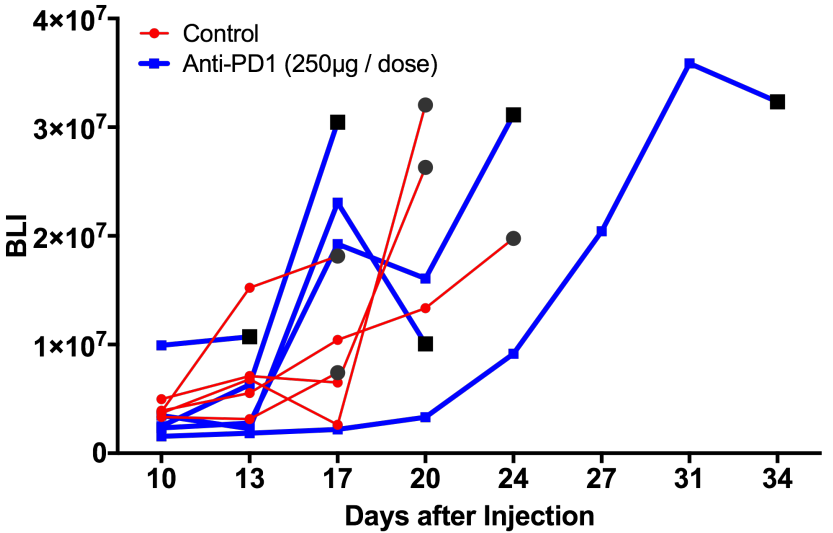

B

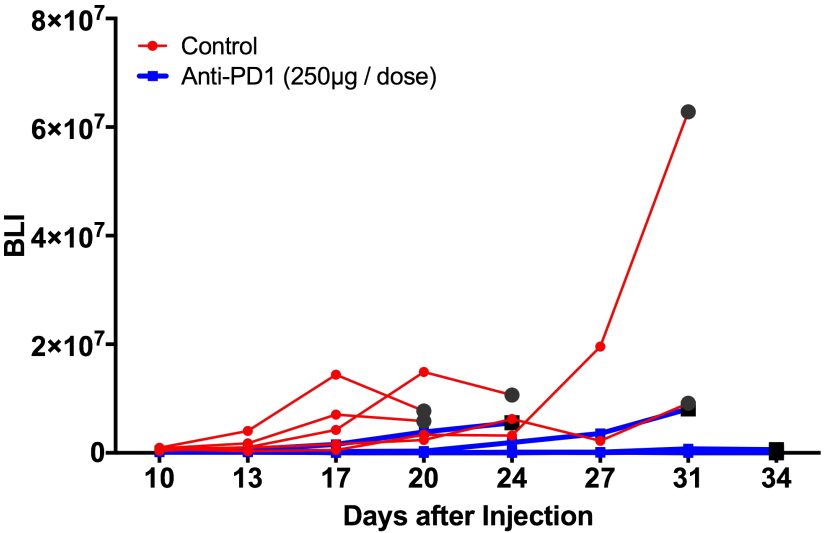

Supplemental Figure 9

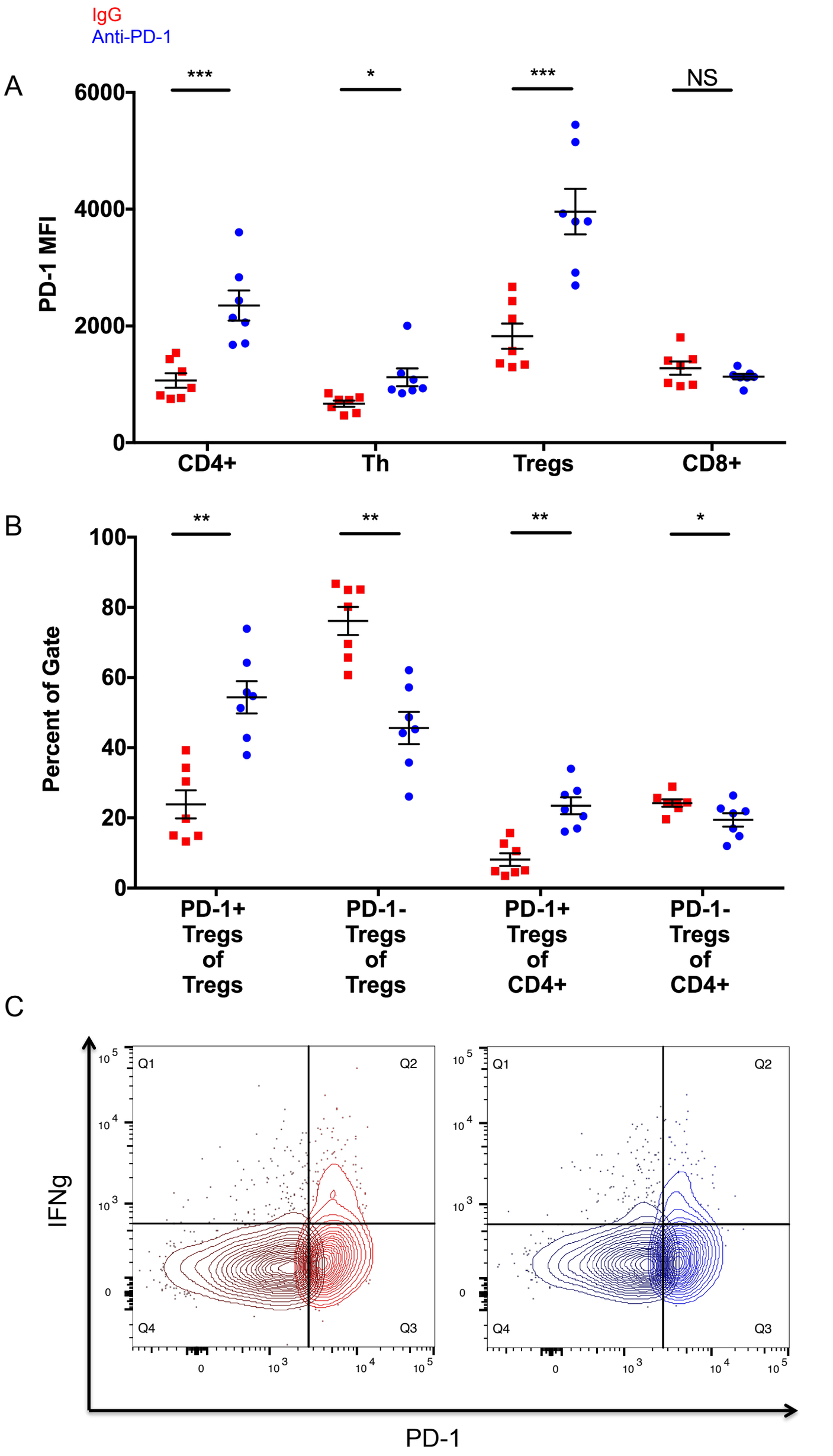

Supplemental Figure 10

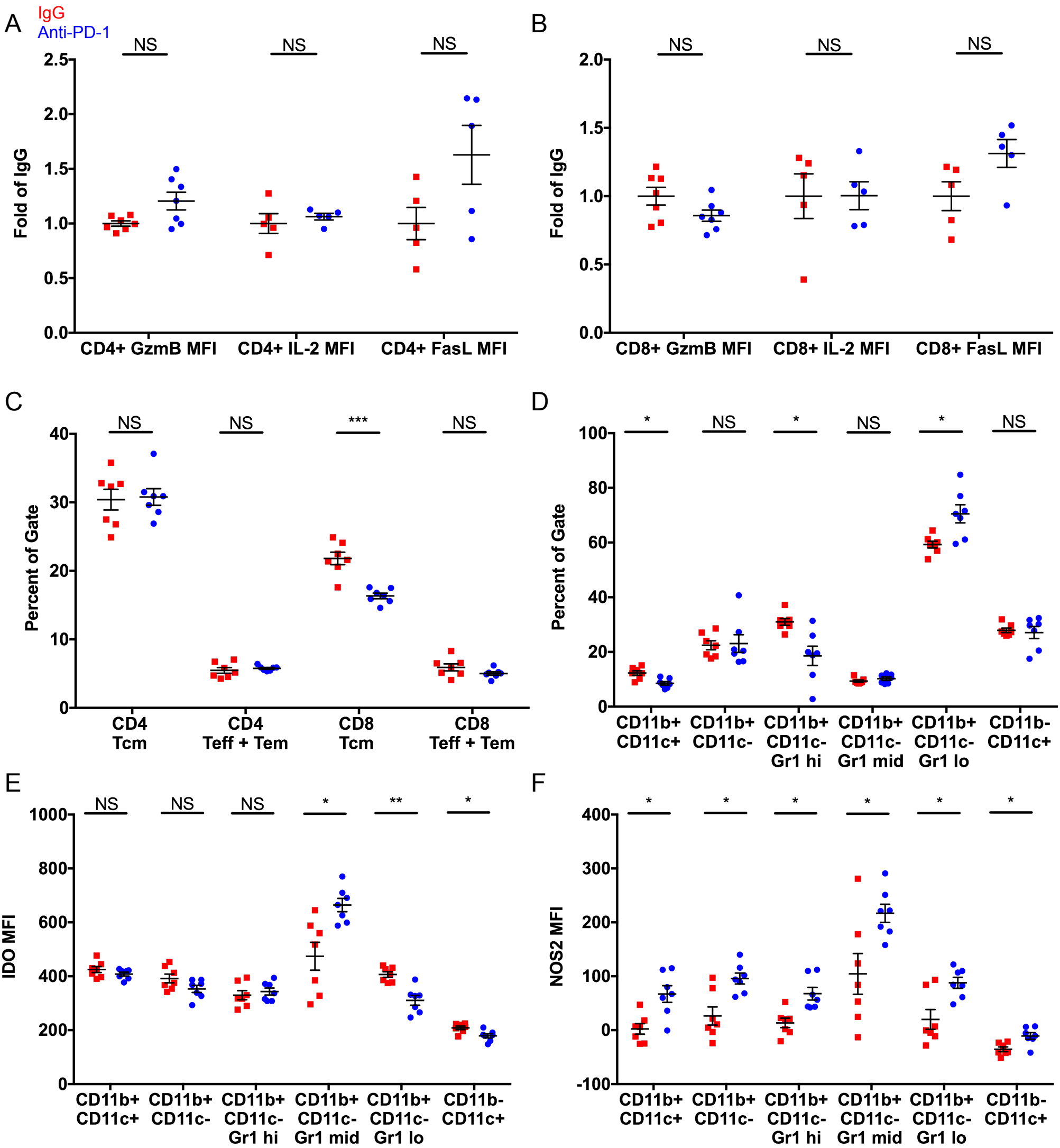

Supplemental Figure 11

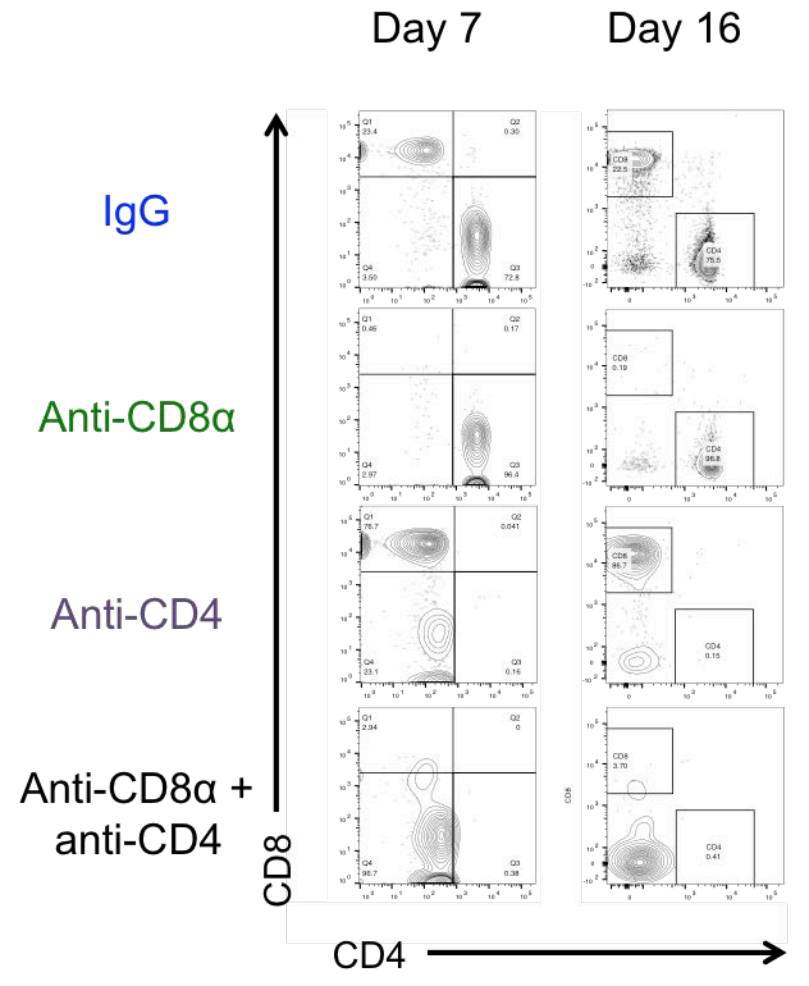

Supplemental Figure 12

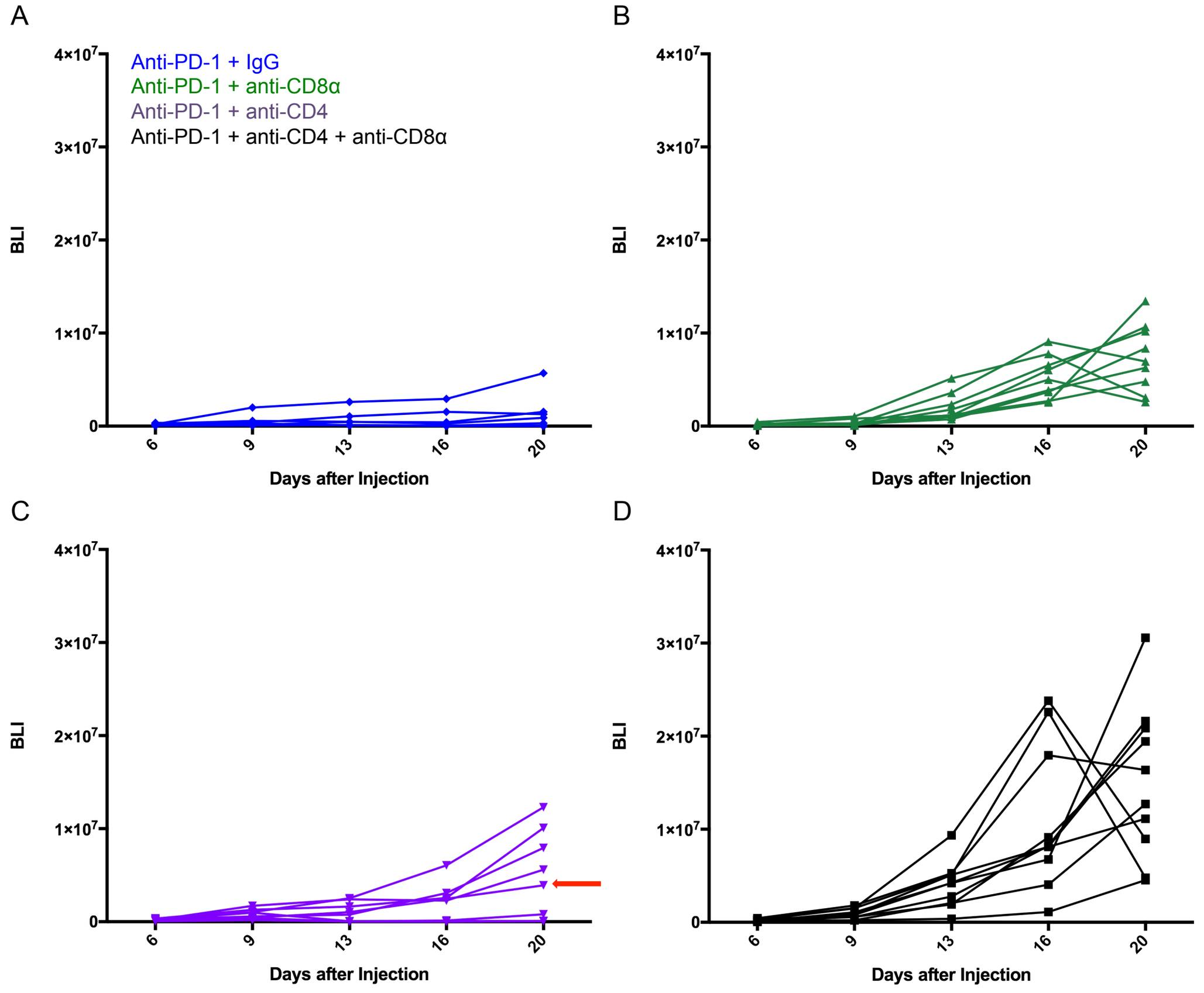

Supplemental Figure 13

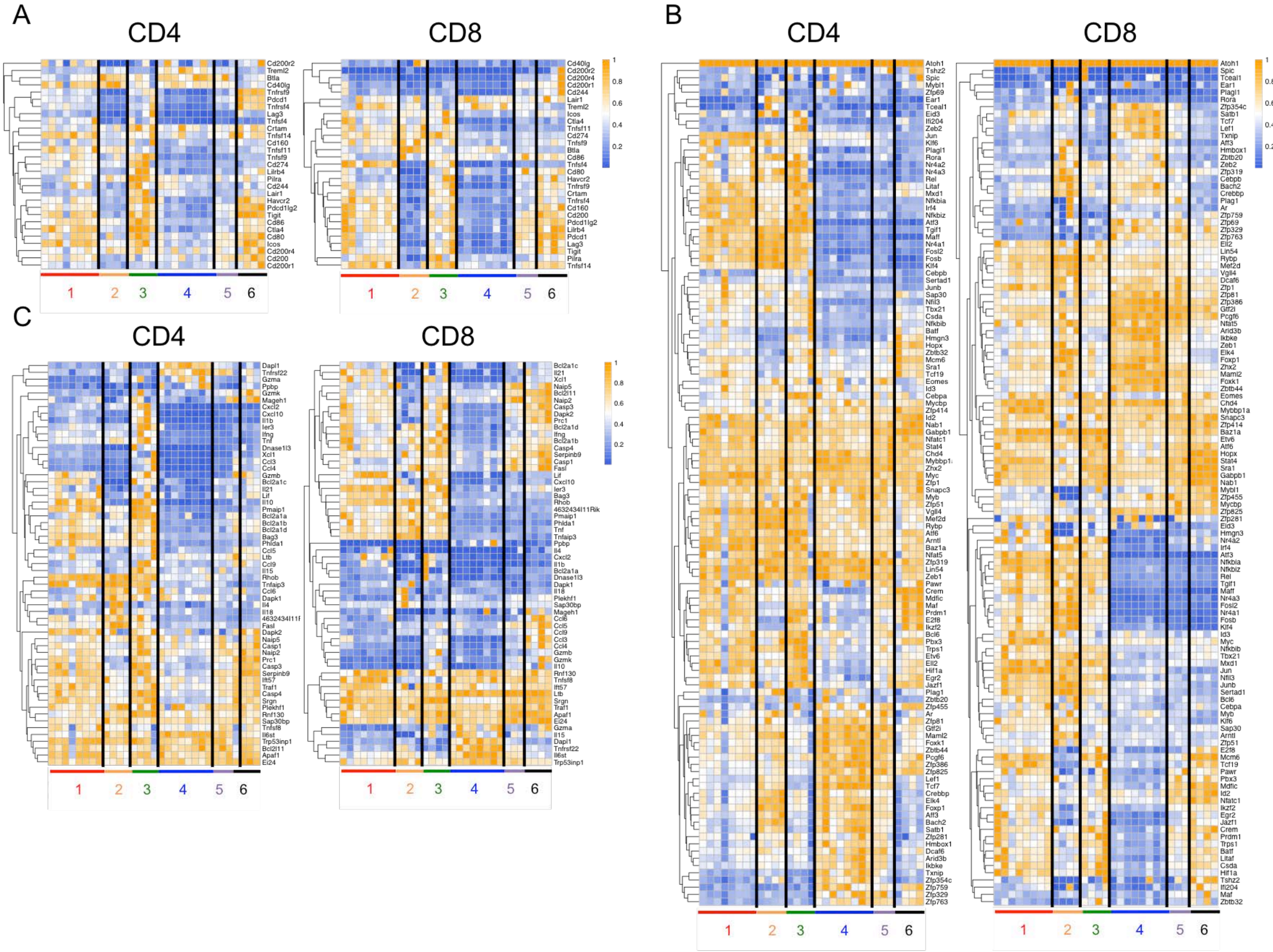

Supplemental Figure 14

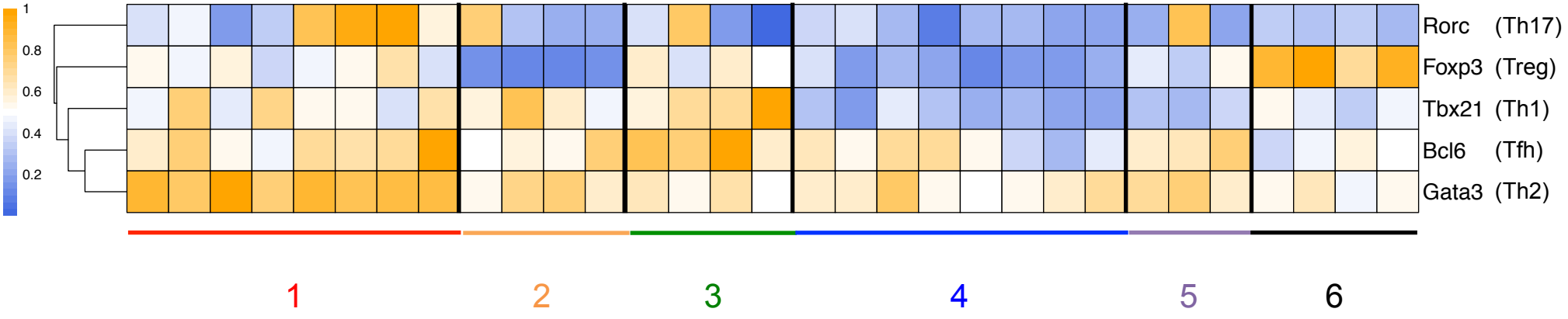

Supplemental Figure 15

CD4

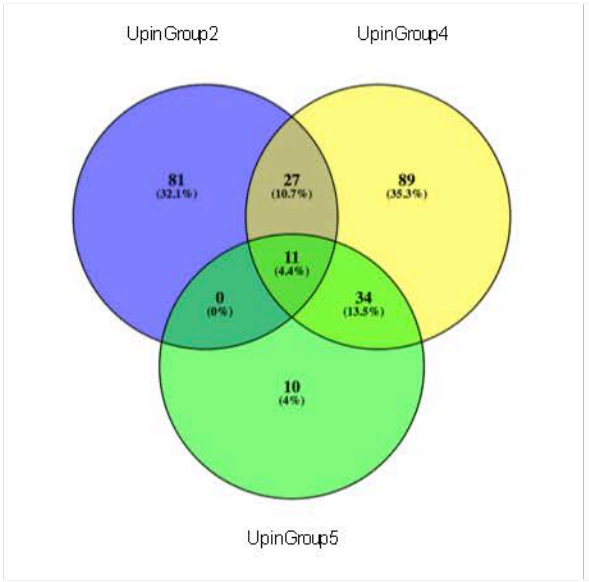

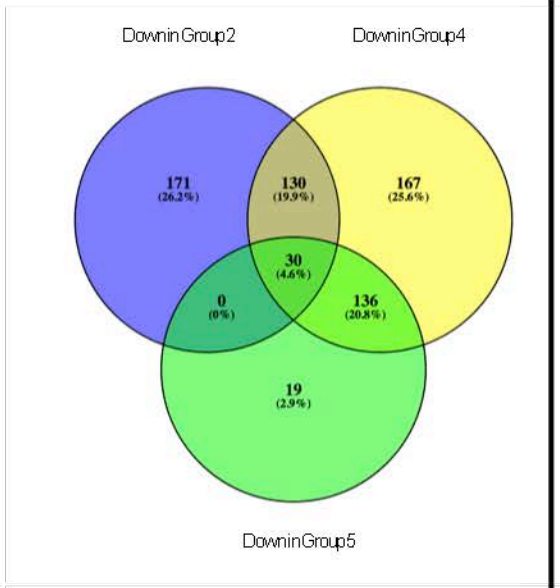

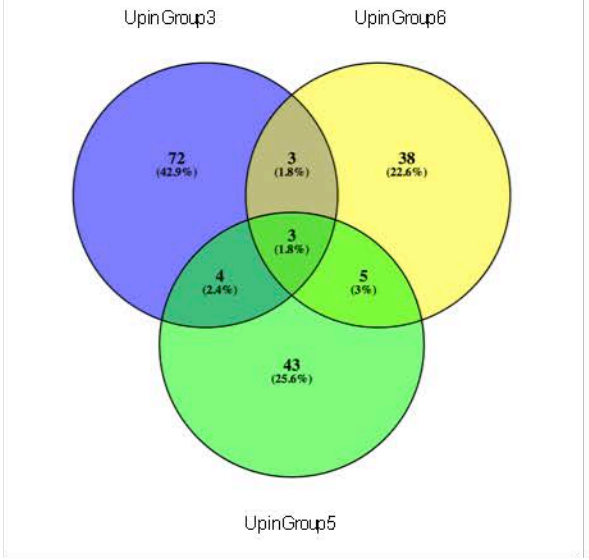

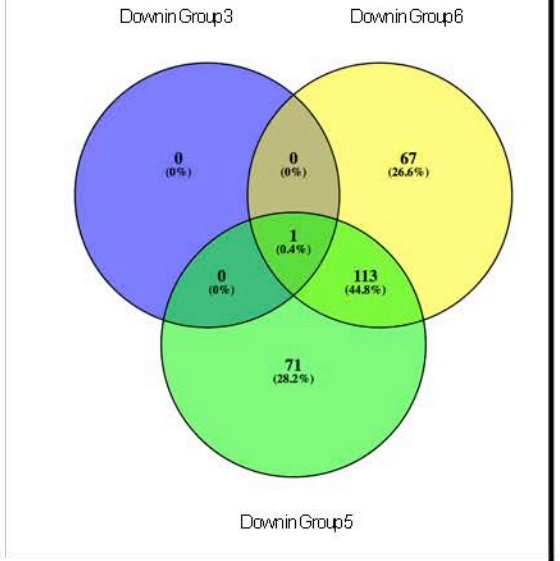

CD8

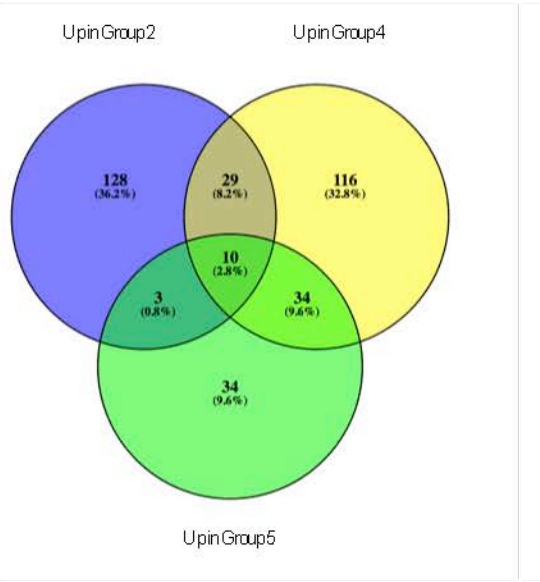

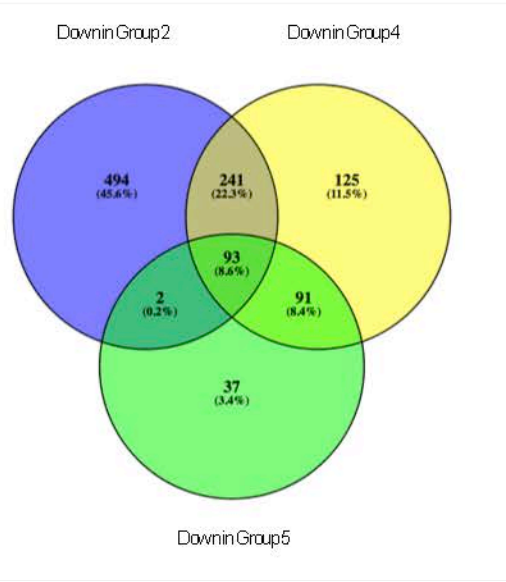

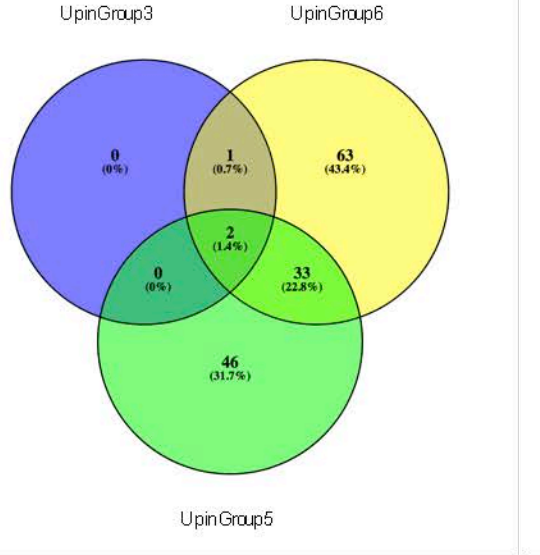

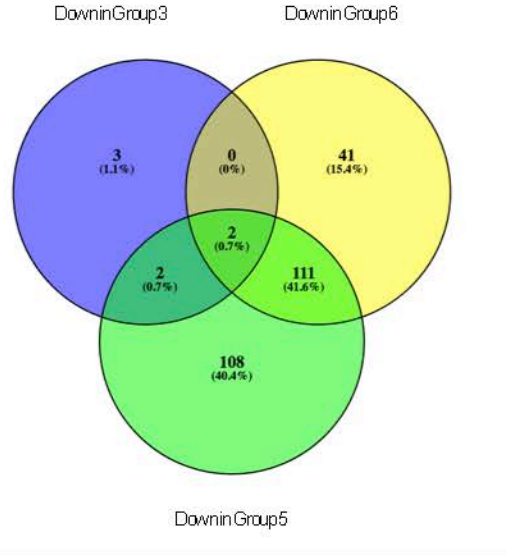

Supplemental Figure 16

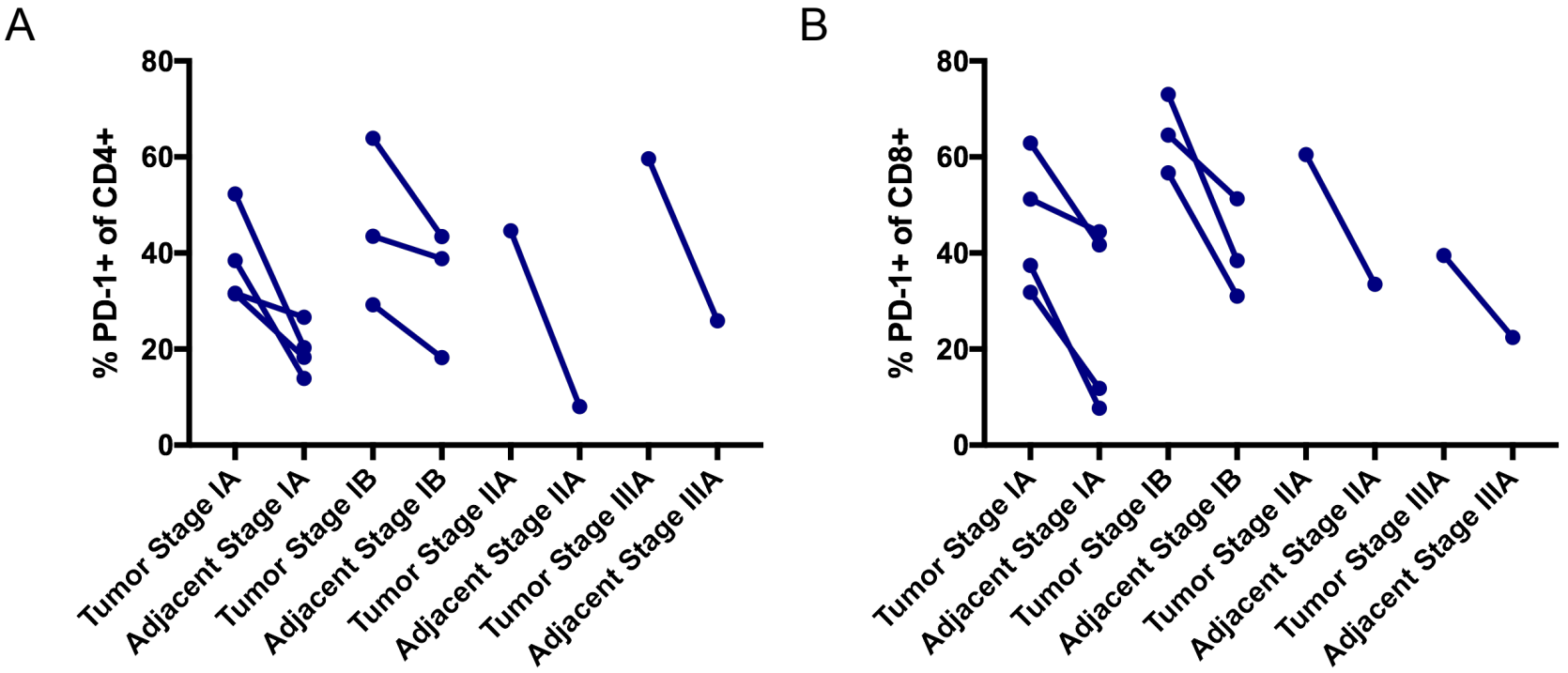

Supplemental Figure 17

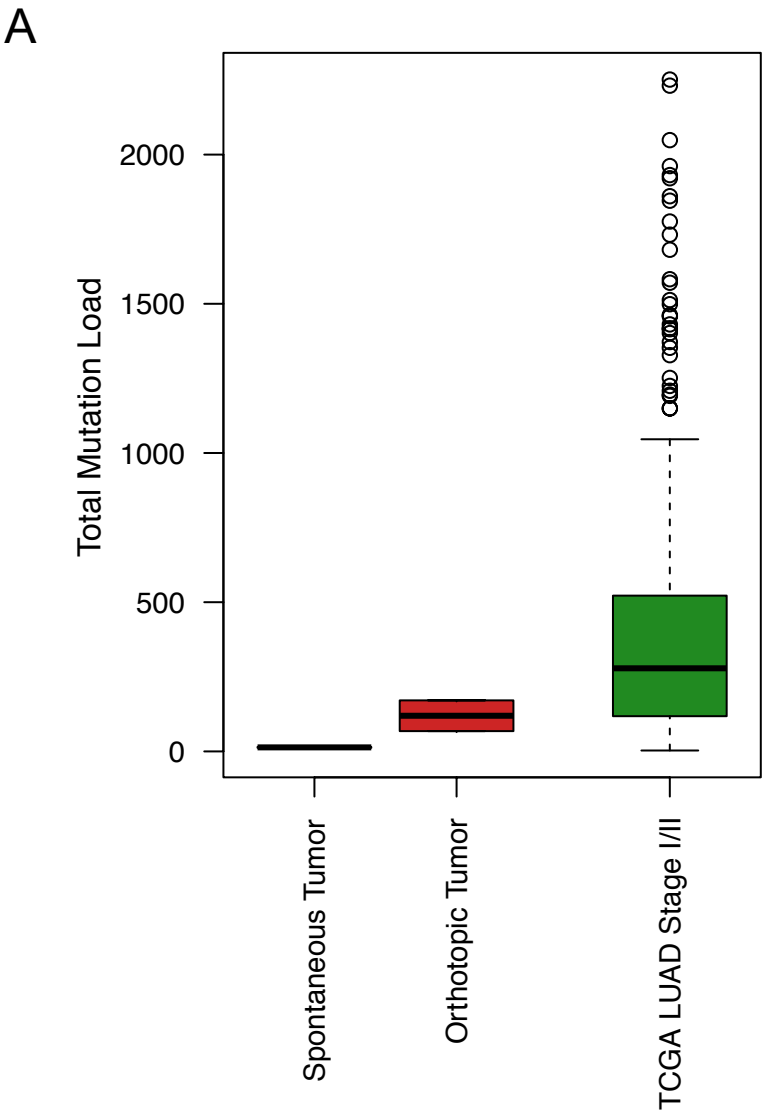

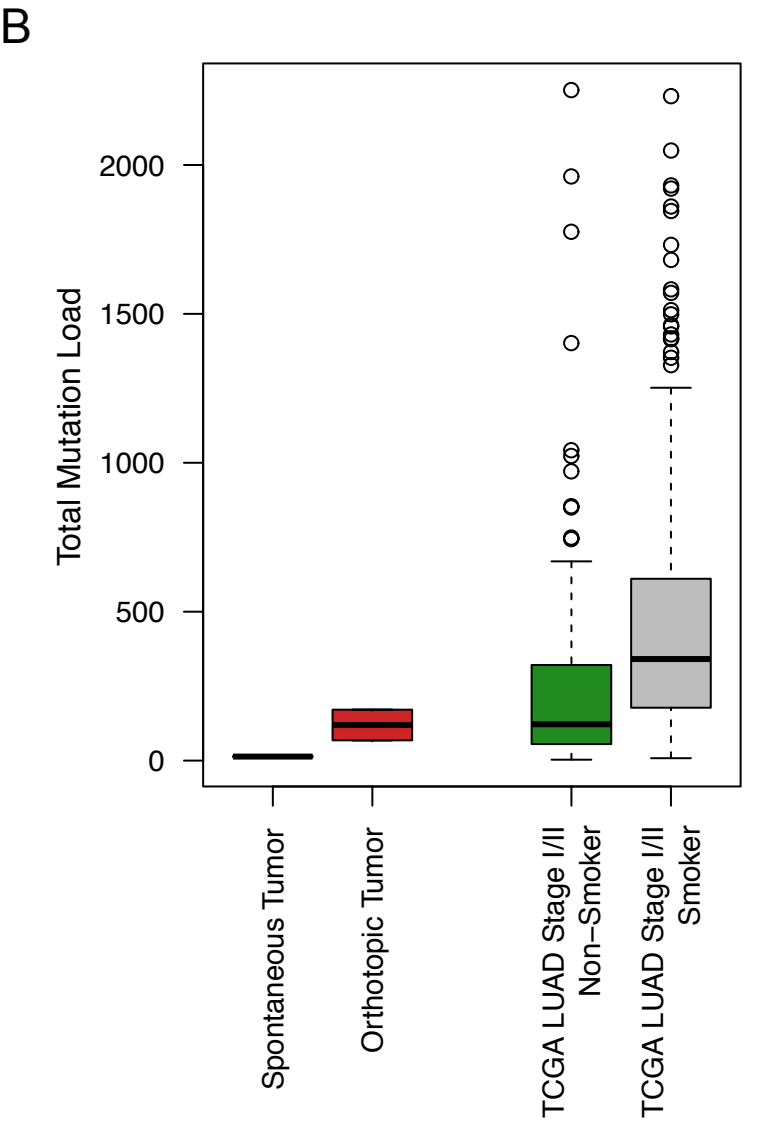

Supplemental Figure 18